Numerical investigation of the high pressure selective catalytic reduction system impact on marine two-stroke diesel engines

Daoyi Lu[a,b,1], Gerasimos Theotokatos[b, 1], Jundong Zhang[a,*], Yuanyuan Tang[a], Huibing Gan[a,b], Qingjiang Liu[c] and Tiebing Ren[d]

a Marine Engineering College, Dalian Maritime University, Dalian 116026, China

b Maritime Safety Research Centre, Department of Naval Architecture, Ocean and Marine Engineering, University of Strathclyde, 100 Montrose Street, Glasgow G4 0LZ, Scotland, UK

c Dalian Shipbuilding Industry co., ltd, Dalian 116000, China

d Dalian Branch, China Classification Society, Dalian 116013, China

***Correspondence information:**

Jundong Zhang

Marine Engineering College, Dalian Maritime University, Dalian 116026, China

E-mail address: zhjundongpaper@163.com

The first author information:

Daoyi Lu

Marine Engineering College, Dalian Maritime University, Dalian 116026, China

E-mail address: ludaoyii@dlmu.edu.cn

The second author information:

Gerasimos Theotokatos

Maritime Safety Research Centre, Department of Naval Architecture, Ocean and Marine Engineering, University of Strathclyde, 100 Montrose Street, Glasgow G4 0LZ, Scotland, UK

E-mail address: gerasimos.theotokatos@strath.ac.uk

[1] These authors contributed equally to this work.

Abstract

After-treatment systems using the selective catalytic reduction (SCR) technology have demonstrated a potential to reduce the nitrogen oxides (NOx) emissions from marine engines by more than 90% with its most typical configurations being the high pressure system (SCR-HP) and the low pressure system (SCR-LP). This study aims to investigate the impact of the SCR-HP system on a large marine two-stroke engine performance parameters by employing thermodynamic modelling. A coupled model of the zero-dimensional type is extended to incorporate the modelling of the SCR-HP system components and the control bypass valve (CBV) block. The CBV control system is modelled based on the exhaust gas minimum temperature set point, which is considered a function of the sulphur content and the exhaust receiver pressure. This model is initially validated against experimental data and subsequently employed to simulate several scenarios representing the engine operation at both healthy and degraded conditions considering the compressor fouling and the SCR reactor clogging. The derived results are analysed to quantify the impact of the SCR-HP system on the investigated engine performance. The SCR system pressure drop and the cylinder bypass valve flow cause an increase of the engine specific fuel oil consumption (SFOC) in the range 0.3 to 2.77 g/kWh. The thermal inertia of the SCR-HP system is mainly attributed to the SCR reactor, which causes a delayed turbocharger response. These effects are more pronounced at low engine loads. This study supports the better understanding of the operating characteristics of marine two-stroke diesel engines equipped with the SCR-HP system and quantification of the impact of the components degradation on the engine performance. Furthermore, it provides insights for the effective shipboard operation of these engines and the SCR-HP system.

Keywords: High pressure selective catalytic reduction (SCR-HP), Marine two-stroke diesel engine, thermodynamic modelling, healthy and degraded operation.

1. Introduction

With over 80% of global trade volume and more than 70% of its value being carried by ships and handled by seaports worldwide **[1]**, maritime transport is widely acknowledged for its key importance to global trade and economy. However, the maritime industry growth resulted in environmental challenges mainly caused by the exhaust emissions of marine engines and the societal need for reducing of the greenhouse gases and other harmful emissions including the nitrogen oxides (NOx), sulphur oxides (SOx), unburnt hydrocarbons and particulate matters **[2,3]**. To reduce the NOx emissions from marine engines, the International Maritime Organisation (IMO) has established limits and identified Emission Control Areas (ECAs) **[4]**. In January 2016, the IMO Tier III regulations for NOx emissions were enforced in North America ECA, whereas it should take effect in Northern Europe ECA including Baltic Sea, North Sea and English Channel in January 2021 **[5,6]**.

To comply with the stricter NOx Tier III emission limits, various NOx reduction technologies for marine diesel engine including selective catalytic reduction (SCR), exhaust gas recirculation (EGR), the use of alternative fuels, operational settings control, direct water injection (DWI), fuel-water emulsion (FWE) and intake air humidification, have been researched, developed and implemented by the engine manufacturers **[7-14]**. The EGR technology can reduce the NOx emissions by up to 40% **[15]**, whereas the SCR technology demonstrated a potential to reduce NOx emissions by more than 90% **[7,16]**. The SCR systems include a catalytic reactor, where the NOx is converted to nitrogen and water vapour by using ammonia as a reducing agent, which is typically produced by the injection of urea-water solution. The reactor catalyst consists of blocks with a large number of channels, providing a large surface area, in which the catalytic process takes place.

The most typical configurations of the SCR system include the high pressure system (SCR-HP) and the low pressure system (SCR-LP) **[17,18]**. The SCR-LP system is installed downstream the engine turbocharger turbine, which provides flexibility in the system installation and has a small impact on the engine performance. However, due to the requirement for a relatively high temperature for the SCR process, additional equipment such as heaters is needed, which renders the SCR-LP system more complicated. In addition， the SCR-LP system cannot normally be used for high sulphur fuels, which are typically used in marine two-stroke engines. In the latter case, an additional SOx scrubber system is required to ensure the compliance with the existing SOx emissions regulations.

The SCR-HP system is installed in the engine high pressure side, i.e., upstream the engine turbocharger turbine. Depending on the engine operating conditions, the exhaust gas temperature before the turbine can reach values 50−175°C higher than the temperature in the low pressure side (downstream turbine). Hence, the SCR-HP system does not require an additional heating device, which renders the SCR-HP system arrangement more compact. However, it is expected to impact the engine performance and transient response due to the SCR components pressure drop, the variation of the exhaust gas temperature caused by the injected urea-water solution evaporation and the reactions taking place in the catalyst surface, as well as the additional thermal and fluid inertias of the exhaust receiver and the SCR catalyst system.

For SCR systems shipboard applications, a considerable number of research studies focused on new catalyst materials **[19-23]**, reaction mechanisms **[24-28]**, chemical reactions modelling **[29-31]** and design optimisation **[34-39]** to improve the efficiency of NOx emissions reduction rather than the SCR system thermal behaviour. **Chen and Wang [40-41]** developed a control-oriented temperature dynamic model for a diesel engine equipped with a complete set of after-treatment systems including Diesel Oxidation Catalyst (DOC), Diesel Particulate Filter (DPF), and Urea-Based Selective Catalytic Reduction (SCR) system. In **Ref. [42]**, the effect of static mixer geometry on flow mixing and pressure drop in marine SCR applications was investigated. **In Ref. [43]**, a simple thermodynamic model of the SCR reactor used to verify that a functional mockup interface (FMI) can be used for co-simulation of embedded SCR control software and for control software development is reported. The output temperature of the

SCR was modelled as the relationship between the reactor throttle valve (RTV) position, the flow through the reactor and the input temperature of the SCR.

Studies investigating the influence of SCR system on the marine two-stroke diesel engines performance are limited. In **Ref. [17]**, the thermal inertia caused by the SCR system on marine two-stroke diesel engine was discussed and appropriate countermeasures were proposed. In **Ref. [44]**, an SCR model predicting the transient thermal response of a SCR-HP system for a Tier III marine two-stroke diesel engine was presented. **Foteinos et al. [45]** presented a coupled model of the marine propulsion plant with an SCR system and studied the response of a direct-drive large marine two-stroke engine with SCR operating in waves. **Zhu et al. [46]** investigated the effects of the scavenging bypass and the turbine exhaust bypass modules on the exhaust gas temperature and pressure of a low-speed marine diesel engine.

The application of the SCR system in marine two-stroke diesel engines is more challenging than respective applications in heavy-duty four-stroke engines due to the demand for a relatively high temperature for the SCR process. At temperature levels below the minimum required temperature, ammonium bisulphate (NH_4HSO_4, hereafter denoted as ABS) is formed, which accumulates in the SCR reactor causing the reactor clogging. Even though the reactor is placed upstream the turbine, the exhaust gas temperature will still be too low at low loads. To increase the temperature, a cylinder bypass branch from the scavenge air receiver to the turbine inlet is required. The bypass air flow is controlled by the cylinder bypass valve (CBV). With the CBV open, the air trapped into the cylinders is reduced, thus, resulting in the exhaust gas temperature increase retaining the temperature above the required level. However, this also increases the engine fuel consumption.

The common failures of marine diesel engines without the SCR system were investigated by simulation in References **[64-66]**. These studies results indicated that the turbocharger degradation has a great impact on engine performance parameters. Thus, it is expected that the turbocharger components degradation will also affect the performance of the SCR-HP system. In addition, the SCR reactor degradation and partial clogging also impacts the engine performance parameters along with the after-treatment system effectiveness.

This study aims at investigating the operation of a marine two-stroke diesel engine with a SCR-HP system and a cylinder bypass valve in order to quantify the impact of the after-treatment system on the engine performance parameters and reveal the interactions between the engine subsystems/components. In addition, a number of engine operating scenarios are investigated using fuels with different sulphur content and considering degraded conditions, in particular, the turbocharger compressor and the SCR reactor partial clogging. This study employs an existing thermodynamic model of the zero-dimensional type that adequately represents the engine operation. This model was extended to incorporate models for the SCR system and the CBV along with its control, for which the minimum temperature set point is calculated as function of the sulphur content and the exhaust receiver pressure. To the best of the authors' knowledge, this is the first study investigating the two-stroke engine along with the SCR system and the CBV with its control system, whilst considering engine components degradation. The analysis presented in this study leads to the better understanding of the involved phenomena in the engine and its components as well as the interactions between the engine components, underlying the critical operating parameters at both healthy and degraded conditions.

The remaining of this study is structured as follow. In **Section 2**, the employed engine model and its extension to incorporate the SCR system model and the CBV block model are described. In **Section 3**, the model validation by comparing with experimentally measured data is discussed. The simulated case studies along with the derived results are presented and discussed in **Section 4**. The last section summarises the main findings and the conclusions drawn from this study.

2. Model Description

2.1 Engine modelling

The zero-dimensional and the mean value approaches are the most widely used for the marine diesel engine modelling mainly because of their low computational effort and capability of achieving satisfactory simulation accuracy **[52-54]**. The mean value models (MVM) require lower computational cost (compared to zero-dimensional models), however they cannot predict the in-cylinder parameters variations. The zero-dimensional models describe the cylinder processes on crank angle basis and can predict the in-cylinder parameters variations. Typically, they represent with sufficient accuracy the engine fuel consumption capturing the cylinder pressure variation, in comparison with the MVMs. Hence, a zero-dimensional modelling approach is adopted in this study, the principles of which are described in **[47]** and **[51]**. The main governing equations are provided in the following sub-sections.

2.1.1 Cylinder processes modelling

The working processes within the engine cylinders include different stages and thermodynamic characteristics. One zone is considered for the case of the cylinder closed cycle, whereas a two-zone approach is assumed for the open cycle as delineated below. The energy conservation provides the following equation for the calculation of the in-cylinder temperature time derivative in each considered zone:

$$\frac{dT_z}{dt} = \frac{1}{m_z c_v}\left(\frac{dQ_f}{dt} + \frac{dm_{sz}}{dt}h_{sz} - \frac{dm_{ze}}{dt}h_{ze} - \frac{dQ_w}{dt} - p_z\frac{dV_z}{dt} - u\frac{dm_z}{dt}\right) \quad (1)$$

where dm_{sz}/dt is the scavenging air mass flow rate entering the cylinder, h_{sz} is the specific enthalpy of scavenging air, dm_{ze}/dt is the exhaust gas mass flow rate exiting the cylinder, h_{ze} is the specific enthalpy of the exhaust gas exiting the cylinder, p_z is the in-cylinder pressure, which can be calculated according to the ideal gas state equation, dV_z/dt is the cylinder volume time derivative, u is the specific internal energy of gas in the cylinder, dm_z/dt is the time derivative of the in-cylinder gas mass, dQ_f/dt is the combustion heat released into the in-cylinder gas, and dQ_w/dt is the heat transfer from the in-cylinder gas to the cylinder walls. The combustion heat release rate and the heat transfer coefficient are calculated by employing the double-Wiebe function **[33]** and the Woschni empirical formula **[32],** respectively**.**

The scavenging process in this study is described by a two-phase, two-zone model **[48-50, 63]**. It assumed that the scavenging process in the first phase is the displacement scavenging, considering one mixing zone and one displacement zone as shown in **Fig. 1(a).** In the second phase of the scavenging period, one mixing zone and one short-circuit zone are considered, as shown in **Fig. 1(b).**

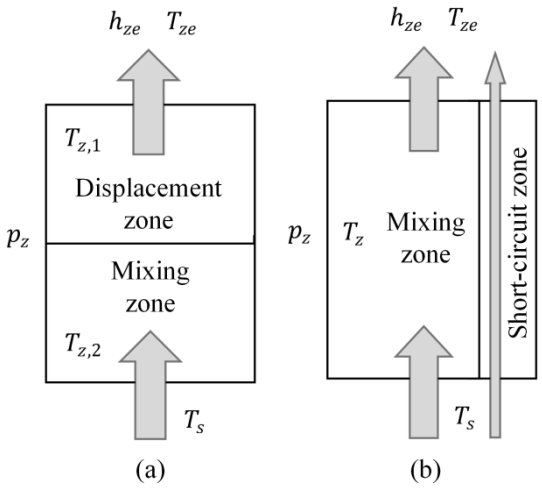

Fig. 1 Schematic diagram of the employed two-phase, two-zone scavenging model

2.1.2 Scavenging air and exhaust gas receivers modelling

The engine receivers are modelled as open thermodynamic systems with a constant volume **[56]**. The mass and energy conservations were considered to derive the equations for the calculation of the receiver working medium mass and temperature time derivatives, respectively.

For multi-cylinder diesel engines, the total mass flow rate exiting the scavenging air receiver is the sum of the mass flow rates entering the engine cylinders. The mass flow rate entering the exhaust gas receiver is the sum of the mass flow rates exiting the engine cylinder. In this study, the heat transfer is only considered in exhaust gas receiver. The pressure of each receiver is calculated according to the ideal gas state equation.

2.1.3 Turbocharger components modelling

Several methods of various complexities are used for investigating the performance of turbocharger components **[57].** The adiabatic nozzle modelling approach **[58]**, which represents the turbine as a nozzle, is employed herein for the calculation of the turbine mass flow rate as function of the turbine pressure ratio and the effective geometric area. The compressor is modelled by employing the steady state compressor map in a digital form. The compressor mass flow rate is calculated by interpolation **[59, 60]** as function of the turbocharger speed. The generated turbine power is calculated according to the flowing equation:

$$P_t = \dot{m}_t c_p T_e \eta_t \left(1 - \Pi_t^{\frac{k-1}{k}}\right) \tag{2}$$

where $\dot{m}_t$ is the turbine mass flow rate, c_p is the exhaust gas specific heat capacity at constant pressure, T_e is the temperature of exhaust gas entering the turbine, η_t is the turbine efficiency, Π_t is the turbine pressure ratio, and k is the ratio of specific heats of the exhaust gas.

The absorbed compressor power is calculated by the following equation:

$$P_c = \dot{m}_c c_p T_a \frac{1}{\eta_c}\left(\Pi_c^{\frac{k-1}{k}} - 1\right) \tag{3}$$

where $\dot{m}_c$ is the compressor mass flow rate, c_p is the air specific heat capacity at constant pressure, T_a is the air temperature at the compressor inlet, η_c is the compressor isentropic efficiency, and Π_c is the compressor pressure ratio.

The air temperature at the compressor outlet is calculated according to the following equation:

$$T_c = T_a \left[1 + \frac{1}{\eta_c}\left(\Pi_c^{\frac{k-1}{k}} - 1\right)\right] \tag{4}$$

The compressor degraded condition is taken into account by considering the compressor isentropic efficiency reduction as reported **[64]**. This reduction is mainly caused by changes in geometry**,** which causes a drop in the power absorbed by the compressor and further affects the performance of the diesel engine. The impact factor κ_c is introduced into the model to simulate compressor degradation as the following equation:

$$\eta_{c,f} = \kappa_c \eta_{c,n} \tag{5}$$

where κ_c represents the degree of compressor degradation, which is set to 0.8 in this study, $\eta_{c,f}$ is the compressor isentropic efficiency in the degraded conditions, $\eta_{c,n}$ is the compressor isentropic efficiency in healthy conditions.

2.2 SCR system modelling

A SCR modelling approach reported in **[44, 45]** is adopted and integrated with the zero-dimensional engine

model. The SCR system is divided into three primary components, namely the vaporizer, the SCR reactor, and the pipe connecting the vaporizer and the reactor. The input parameters considered by the model are shown in **Fig. 2** and include the exhaust gas temperature T_e, the exhaust gas pressure p_e, the exhaust gas mass flow rate $\dot{m}_e$ and the urea mass flow rate $\dot{m}_{urea}$. In addition, the geometric characteristics of each component (vaporizer, pipe, and reactor) are required as input to the model.

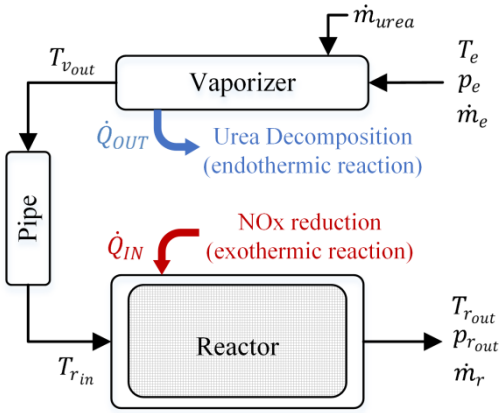

Fig. 2 SCR system modelled components

2.2.1 Vaporizer modelling

The vaporizer is considered as a volume containing exhaust gas, in which the urea solution is injected. The energy rate flowing in the vaporizer mainly consists of five parts, namely $\dot{Q}_{exh_{in}}$, $\dot{Q}_{exh_{out}}$, $\dot{Q}_{g\to w}$, $\dot{Q}_{env}$, and $\dot{Q}_{ch_{vap}}$, which are shown in **Fig. 3 [44]**.

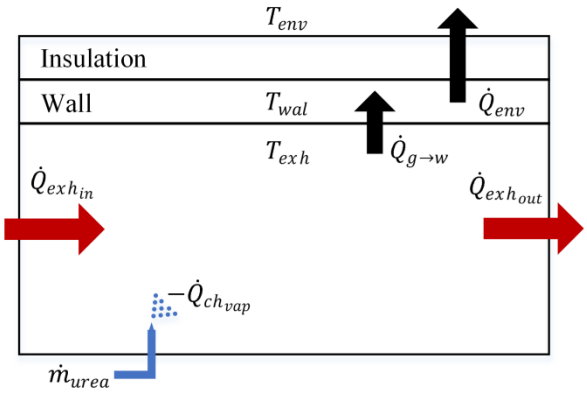

Fig. 3 Energy flow in the vaporizer

$\dot{Q}_{exh_{in}}$ and $\dot{Q}_{exh_{out}}$ represent the energy rate of the exhaust gas entering and exiting the vaporizer, which are described by the following equations:

$$\dot{Q}_{exh_{in}} = \dot{m}_{exh} c_{exh} T_{exh_{in}} \tag{6}$$

$$\dot{Q}_{exh_{out}} = \dot{m}_{exh} c_{exh} T_{exh_{out}} \tag{7}$$

where $\dot{m}_{exh}$ is the mass flow rate of the exhaust gas entering the vaporizer volume, c_{exh} is the exhaust gas specific heat capacity at constant pressure, $T_{exh_{out}}$ is the temperature of the exhaust gas exiting the vaporizer, and $T_{exh_{in}}$ is the temperature of the exhaust gas entering the vaporizer.

$\dot{Q}_{g\to w}$ considers the convective and radiative heat losses from the exhaust gas to the vaporizer wall, which can be calculated according to the following equation:

$$\dot{Q}_{g\to w} = \eta_{gw} A_{gw}(T_{exh} - T_w) + \sigma \varepsilon_{g\to w} A_{gw}(T_{exh}^4 - T_w^4) \tag{8}$$

where η_{gw} is the convective heat transfer coefficient between the exhaust gas and the vaporizer wall, A_{gw} is the inner surface area of the wall in contact with the gas, σ is Stefan–Boltzmann constant, $\varepsilon_{g\to w}$ is emissivity between the exhaust gas and the wall, T_{exh} is the temperature of the exhaust gas in the vaporizer volume, and T_w is the wall temperature.

$\dot{Q}_{env}$ represents the heat losses from the wall to the environment, which is obtained by the following equation:

$$\dot{Q}_{env} = \frac{T_w - T_{amb}}{R_w + R_{ins} + R_{env}} \tag{9}$$

where T_{amb} is the ambient temperature, R_{wal} and R_{ins} are thermal resistances of the conduction through wall and insulation layers, respectively, and R_{env} is the thermal resistance due to convection between the external wall and the environment.

The equations for the time derivatives of the exhaust gas and wall temperature in the vaporizer can be obtained using the conservation of energy:

$$\frac{dT_{exh}}{dt} = \frac{1}{m_{exh} c_{exh}} \left(\dot{Q}_{exh_{in}} - \dot{Q}_{exh_{out}} - \dot{Q}_{g\to w} - \dot{Q}_{ch_{vap}} \right) \tag{10}$$

$$\frac{dT_w}{dt} = \frac{1}{m_w c_{wal}} \left(\dot{Q}_{g\to w} - \dot{Q}_{env} \right) \tag{11}$$

where m_{exh} is the exhaust gas mass, which is calculated using the ideal gas state equation, m_w is the mass of the vaporizer, c_w is the specific heat capacity of the wall, and $\dot{Q}_{ch_{vap}}$represents the energy loss due to the endothermic reaction of the urea evaporation and decomposition, which is calculated by the following equation **[44]**:

$$\dot{Q}_{ch_{vap}} = m_{exh} c_{exh} (0.034\, L + 240 \dot{m}_{urea}) \tag{12}$$

where L denotes the engine load percentage (0–100), $\dot{m}_{urea}$ is the urea mass flow rate (kg/s), which is found to vary linearly with engine load according to the following equation **[44]**:

$$\dot{m}_{urea} = \alpha_{urea} (0.00023\, L + 0.004) \tag{13}$$

where α_{urea} is the model calibration factor that depend on the engine type.

In this study, the volume of the pipe is merged into the volume of the vaporizer, and the gas temperature change in the pipe is no longer calculated separately, which can reduce the amount of model calculations. Since the material and the adiabatic heat treatment of the pipe is the same as that of the vaporizer, and endothermic or exothermic reactions in the pipe are not expected to take place, the calculation accuracy of the model will not be affected. Hence, the exhaust gas reactor inlet temperature is the same as the vaporizer outlet temperature.

2.2.2 SCR reactor model

The SCR reactor contains the catalytic reduction material, which will affect the energy transfer in the SCR reactor. The energy flow in the SCR reactor mainly includes seven parts, namely $\dot{Q}_{exh_{in}}$, $\dot{Q}_{exh_{out}}$, $\dot{Q}_{g\to w}$, $\dot{Q}_{g\to c}$, $\dot{Q}_{c\to w}$, $\dot{Q}_{env}$, and $\dot{Q}_{ch_{rea}}$, which are shown in **Fig. 4 [44]**.

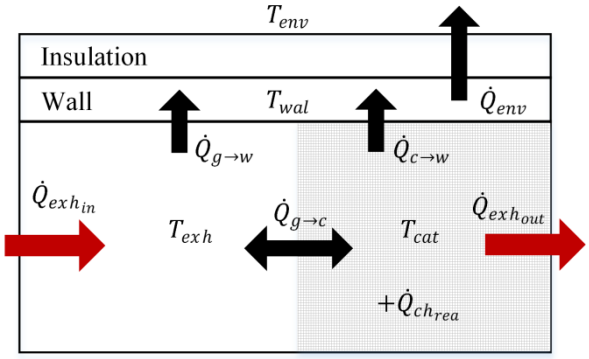

Fig. 4 Energy flow in the SCR reactor

$\dot{Q}_{exh_{in}}$ and $\dot{Q}_{exh_{out}}$ respectively represent the energy rate of the exhaust gas entering and exiting the SCR reactor, which is calculated as **Equation (6) and (7)**.

$\dot{Q}_{g\to w}$ represents convective and radiative losses from the exhaust gas to the wall, which can be calculated as the **Equation (8)**.

$\dot{Q}_{g\to c}$ represents the convective and radiative heat losses from the exhaust gas to the catalyst block, which can be calculated according to Newton's law of cooling and Stefan-Boltzmann law:

$$\dot{Q}_{g\to c} = \eta_{gc} A_{gc}(T_{exh} - T_{cat}) + \sigma \varepsilon_{g\to c} A_{gc}(T_{exh}^4 - T_{cat}^4) \tag{14}$$

where η_{gc} is the convective heat transfer coefficient between the exhaust gas and the catalyst block, $\varepsilon_{g\to c}$ is emissivity between the exhaust gas and the catalyst block, T_{cat} is the catalyst block temperature, and A_{gc} is the total catalyst surface area in contact with the exhaust gas, which is calculated by the equation below:

$$A_{gc} = A_{spec} V_{cat} \tag{15}$$

where V_{cat} is the catalyst volume, and A_{spec} is the specific surface area which is a characteristic catalyst value.

$\dot{Q}_{c\to w}$ represents the heat flow from the catalyst block to the reactor wall through conduction and is calculated according to the following equation:

$$\dot{Q}_{c\to w} = \frac{T_{cat} - T_w}{R_{c\to w}} \tag{16}$$

where $R_{c\to w}$ is the thermal resistance for conductive heat transfer between the catalyst block and the wall.

$\dot{Q}_{env}$ is the heat transfer rate from the wall to the environment, which is obtained by **Equation (9)**.

The following equations for the calculation of the time derivatives of the exhaust gas, wall temperature and the catalyst block in the SCR reactor were derived by using the energy conservation:

$$\frac{dT_{exh}}{dt} = \frac{1}{m_{exh} c_{exh}} \left(\dot{Q}_{exh_{in}} - \dot{Q}_{exh_{out}} - \dot{Q}_{g\to w} - \dot{Q}_{g\to c} + \dot{Q}_{ch_{rea}}\right) \tag{17}$$

$$\frac{dT_w}{dt} = \frac{1}{m_{wal} c_{wal}} \left(\dot{Q}_{g\to w} + \dot{Q}_{c\to w} - \dot{Q}_{env}\right) \tag{18}$$

$$\frac{dT_{cat}}{dt} = \frac{1}{m_{cat} c_{cat}} \left(\dot{Q}_{g\to c} - \dot{Q}_{c\to w}\right) \tag{19}$$

where m_{cat} is the mass of the catalyst block, c_{cat} is the specific heat capacity of the catalyst block, and $\dot{Q}_{ch_{rea}}$ represents the energy added to the gas due to the exothermic SCR reactions. This heat rate is calculated according to the following equation **[44]**:

$$\dot{Q}_{ch_{rea}} = m_{exh} c_{exh} (0.07L + 78\dot{m}_{urea}) \quad (20)$$

The exhaust gas flow through the cells of the catalyst block is treated as laminar, and the pressure drop per unit length is calculated by using the following Hagen–Poiseuille equation **[61]**:

$$\Delta p_{SCR} = \frac{28.5}{d_h^2} \alpha_n L_{cat} \mu v \quad (21)$$

where α_n is a correction factor, μ is the exhaust gas dynamic viscosity that is a function of the temperature, v is the velocity of the exhaust gas through the effective area of catalyst block, L_{cat} is the length of catalyst block, and d_h is the hydraulic diameter of each catalyst cell.

2.2.3 SCR reactor degradation model

The SCR-HP system component degradation considerably affects the engine response **[17]**. The SCR catalyst elements will gradually lose their ability to reduce the NOx emissions. The catalyst lifetime depends on several parameters including the engine load, the operational time, the employed fuel, the exhaust gas composition and temperature as well as the catalyst material. To maintain the required reactor efficiency, the catalyst elements should be replaced periodically according to the requirements of the catalyst supplier. In addition, incomplete combustion products (such as carbon deposits contained in the exhaust gas) and the ABS (formed at low temperatures) accumulate in the reactor catalyst block causing its clogging, which increases the SCR-HP system components pressure drop (losses), thus affecting the engine performance and transient response.

The reactor degradation is investigated by simulation to quantify its impact on diesel engine performance. The factor κ_{SCR} is introduced into the SCR-HP system model to simulate the impact of the reactor clogging on the pressure drop of the SCR-HP system. Hence, the correction factor in Equation **(21)** is replaced by the following factor:

$$\alpha_f = \kappa_{\mathrm{SCR}} \alpha_n \quad (22)$$

where κ_{SCR} represents the degree of the catalyst block clogging and is set to 2 in this study, whereas α_n is the correction factor of Equation **(21)** at normal operating conditions of the SCR-HP system (without clogging).

2.3 Cylinder bypass valve (CBV) block modelling

This section describes the modelling of the CBV block to calculate the CBV opening ϕ_{CBV}, and the cylinder bypass valve air flow rate $\dot{m}_{CB}$ providing as input the setting value of the required minimum temperature T_{set}. The model also calculates the turbine inlet temperature $T_{t_{in}}$. The function diagram of the CBV block is shown in **Fig. 5**.

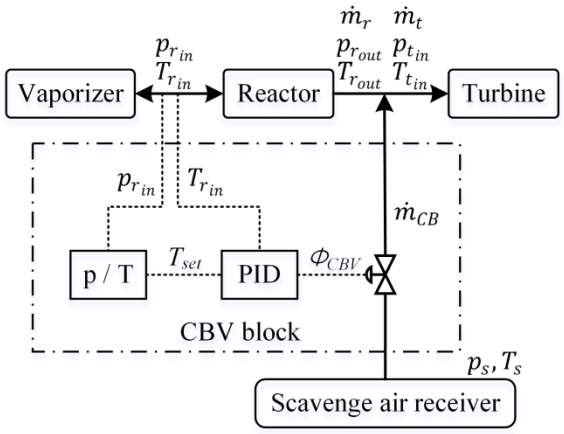

Fig. 5 Function diagram of CBV block model

2.3.1 Minimum temperature setting

Previous studies typically considered fixed the required minimum temperature for the effective operation of the SCR system in marine two-stroke marine diesel engines. The values of 300°C and 320°C were considered for the exhaust gas minimum temperature in **Ref. [45]** and **[46]**, respectively, whereas the minimum temperature was considered 200°C for the marine four-stroke diesel engine reported in **Ref. [62]**. In fact, when the fuel sulphur content is equal or less than 0.1%, a temperature of approximately 310°C would be sufficient. At low exhaust gas pressure, the required minimum temperature must be lower. The minimum temperature required to avoid the formation of ABS can be estimated as function of the fuel sulphur content and the exhaust gas pressure according to **Fig. 6**, which was adapted from **[59]**. The high pressure curve (4.0 bar) and the low pressure curve (1.5 bar) correspond to the typical values of the exhaust receiver pressure for marine two-stroke engines operating at high and at low loads, respectively.

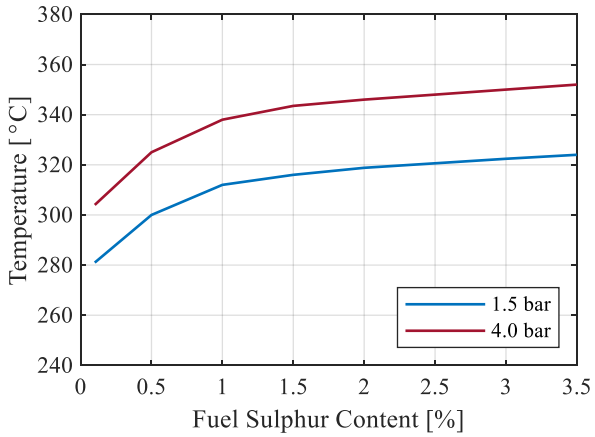

Fig. 6 Required minimum temperatures for SCR as function of the sulphur content and exhaust gas pressure

It is assumed that the required minimum temperature for the normal SCR system operation has a linear relationship with the exhaust gas pressure in the case of a fuel with a specific sulphur content. Hence, the required minimum exhaust gas temperature is calculated according to the following equation:

$$T_{set} = \frac{(p_{r_{in}} - p_L)(T_H - T_L)}{p_H - p_L} + T_L \tag{23}$$

where T_{set} is the setting value of the required minimum temperature, $p_{r_{in}}$ is the pressure of the exhaust gas

entering the SCR reactor, p_L is the exhaust receiver pressure at low load, p_H is the exhaust receiver pressure at high load, T_L is the required minimum temperature corresponding to p_L, T_H is the required minimum temperature corresponding to p_H.

The pressure/temperature (P/T) module shown in **Fig. 5** is used for the T_{set} calculation. This module uses as input the $p_{r_{in}}$ as well as the p_L, p_H, T_L, T_H corresponding to 0.1% sulphur fuel (low sulphur (LS) fuel) and 3.5% sulphur fuel (high sulphur (HS) fuel) estimated from **Fig. 6**. The estimated values of the p_L, p_H, T_L, T_H for LS and HS fuels are summarised in **Table 1**. The temperature response will be delayed as a result of possible delay in the CBV control and the thermal delay of the engine and its SCR system. To prevent the reactor inlet temperature from reducing below the required minimum temperature threshold due to these delays, the P/T module set the T_{set} 5℃ greater than the values corresponding to the calculations according to Table 1.

Table 1 P/T module input parameters

	p_L [bar]	p_H [bar]	T_L [℃]	T_H [℃]
LS Fuel	1.5	4.0	281	304
HS Fuel	1.5	4.0	324	352

2.3.2 CBV control and parameter calculation

The proportional-integral-differential (PID) module shown in **Fig. 5** is used for the adjustment of the required exhaust gas minimum temperature by controlling the CBV opening, which is the output of this module. The input of the PID module is the setting value of the required minimum temperature T_{set} as described in the previous section and the reactor inlet temperature $T_{r_{in}}$. The following equation is employed for the calculation of the CBV opening:

$$\phi_{CBV} = K_p e(t) + \frac{K_i}{T_i}\int_0^t e(t)dt + K_d T_d \frac{de(t)}{dt} \tag{24}$$

where K_p, K_i and K_d are the proportional, integral and derivative gains respectively, and $e(t)$ is the error value defined by the following equation:

$$e(t) = T_{set} - T_{r_{in}} \tag{25}$$

The mass flow of air bypassed from the cylinder $\dot{m}_{CB}$ is calculated by the following equation **[46]**:

$$\dot{m}_{CB} = \phi_{CBV}\dot{m}_{sz} \tag{26}$$

where $\dot{m}_{sz}$ is the scavenge air mass flow rate.

The exhaust gas temperature at the turbine inlet is calculated by considering the mixing of exhaust gas and cylinder bypass air as an adiabatic mixing process. The application of the energy conservation provides the following equation for the turbine inlet temperature calculation **[67]**:

$$T_{t_{in}} = \frac{\dot{m}_{CB}c_{p_s}T_s + \dot{m}_r c_{p_r}T_{r_{out}}}{\dot{m}_t c_{p_t}} \tag{27}$$

where $T_{t_{in}}$ is the turbine inlet temperature, c_{p_s}, c_{p_r} and c_{p_t} are the specific heat capacity at constant pressure of the reactor outlet gas, the cylinder bypassed air and the turbine inlet gas, respectively, T_s is the scavenging air temperature, $T_{r_{out}}$ is the reactor outlet temperature, $\dot{m}_r$ is the reactor mass flow rate and, $\dot{m}_t$ is the turbine mass flow rate, which is calculated by the following equation:

$$\dot{m}_t = \dot{m}_{CB} + \dot{m}_r \tag{28}$$

2.4 Engine integrated model

The integrated model of the marine two-stroke diesel engine with the SCR-HP system and the CBV block was developed in the Simulink environment. The block diagram of the engine integrated model is shown in **Fig. 7**. Each block corresponds to a component of the modelled diesel engine. The "cylinders" block consists of six blocks (one for each engine cylinder). It should be noted that the SCR system operation can be cut off by using the Reactor Sealing Valve (RSV). When RSV is closed, the exhaust gas is directly forwarded to the turbine through the Reactor Bypass Valve (RBV).

The ode2 (Heun) solver based on the improved Euler formula is used in the Simulink model. A fixed step approach was employed with the time step set to 0.002 s. To facilitate the management of the model initial parameters, all the initial parameters are stored in file, which is called at the initial step of the Simulink model.

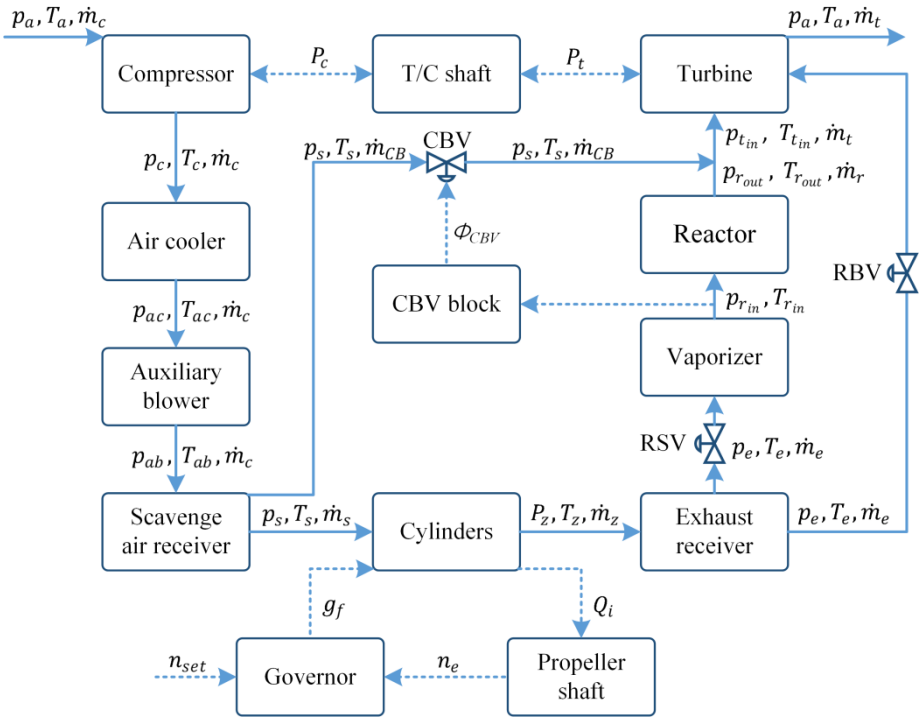

Fig.7 Block diagram of the engine integrated model

3. Model validation

3.1 Engine model validation

The marine two-stroke electronically controlled diesel engine MAN B&W 6S50ME-C8.2 was selected for investigation in this study. The engine main characteristics at the Maximum Continuous Rating (MCR) point are presented in **Table 2**.

Table 2 Engine main characteristics

Parameters	Values
Cylinder number [-]	6
Cylinder diameter [m]	0.5
Stroke [m]	2
Power at MCR [kW]	8280

Speed at MCR [rpm]	127
Pmax at MCR [MPa]	17
Firing order [-]	1-5-3-4-2-6

The engine model was calibrated and validated at 25%, 50%, 75% and 100% load using the engine test data. The simulation results are shown in **Fig. 8 and Fig. 9**. For all the engine parameters, the relative percentage errors between the simulation results and the measured data were found to be less than ±2.4%. This denotes that the model can predict with sufficient accuracy the engine performance parameters and therefore, it can be employed with fidelity to investigate the scenarios investigated in this study.

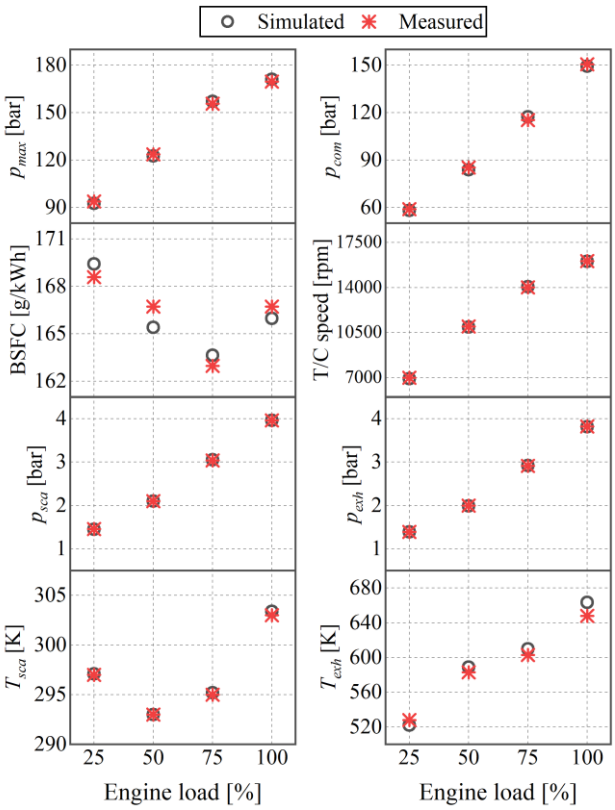

Fig.8 Simulation results and comparison with respective measured data

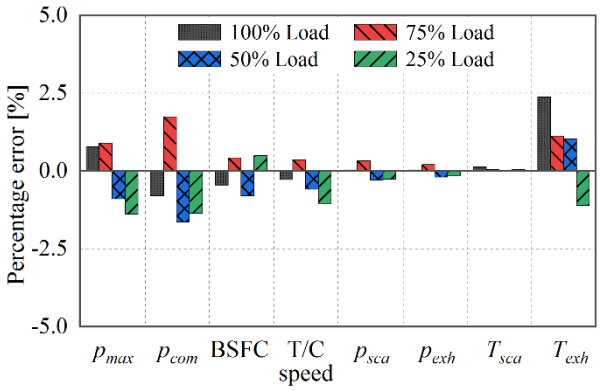

Fig.9 Relative percentage errors between predicted values and measurements

3.2 SCR system model validation

In this section, the SCR system model validation is presented. The main geometric characteristics of the SCR system are adopted from the references **[44] [45]** and are shown in **Table 3**.

Table 3 SCR main characteristics

Parameters	Values
Vaporizer	
Length [m]	5.68
Diameter [m]	0.85
Insulation thickness [m]	0.125
Insulation thermal conductivity [W/mK]	0.15
Specific heat capacity [J/kgK]	600
Pipe (connecting vaporizer and reactor)	
Length [m]	3.41
Diameter [m]	0.54
Insulation thickness [m]	0.125
Insulation thermal conductivity [W/mK]	0.15
Specific heat capacity [J/kgK]	600
Reactor	
Length [m]	6
Diameter [m]	2.54
Insulation thickness [m]	0.125
Insulation thermal conductivity [W/mK]	0.15
Specific heat capacity [J/kgK]	600
Catalyst volume [m^3]	8.02
Catalyst mass [kg]	3500
Catalyst specific area [m^2/m^3]	698
Catalyst specific heat capacity [J/kgK]	1020

Due to the influence of the endothermic and exothermic reactions in the SCR system, the thermodynamic properties of the exhaust gas flowing through the SCR system will significantly vary. The endothermic reaction of urea decomposition in the vaporizer causes the temperature of the exhaust gas flowing through the vaporizer to decrease. The exothermic catalytic reduction reaction in the reactor increases the temperature of the exhaust gas flowing through the reactor. The temperature changes of the exhaust gas flowing through the vaporizer and the reactor at 25%, 50%, 75% and 100% loads are validated against the measurement data reported in reference **[44]**. The coupled model is used as a validation platform for the thermodynamic performance of the SCR system model.

The simulation results are shown in **Table 4**, where $T_{v_{out}}$ is the vaporizer outlet temperature (the reactor inlet temperature $T_{r_{in}}$), $T_{r_{out}}$ is the reactor outlet temperature. The exhaust gas temperature decrease ΔT_v in the vaporizer is found to be around 2–6 K, while the exhaust gas temperature increase ΔT_r in the reactor is around 5–17 K depending on engine load. In the reference **[44]**, the temperature reduction of the exhaust gas in the vaporizer is around 2–7 K, whilst the temperature increase in the reactor is around 4–17 K depending on engine load. It was deduced that the derived simulation results of the SCR system performance parameters are in agreement with the measurement data reported in **[44]**. This finding confirms the fidelity of the developed model allowing for its use for the investigated cases presented in the following section.

Table 4 Exhaust gas temperature changes through the SCR system components

Load [%]	$\dot{m}_e$ [kg/s]	p_e [bar]	T_e [K]	$T_{v_{out}}$ [K]	ΔT_v [K]	$T_{r_{out}}$ [K]	ΔT_r [K]
25	6.48	1.37	543.7	514.2	−2.5	545.7	4.5
50	10.68	2.00	602.7	599.6	−3.1	607.4	7.8
75	15.51	2.97	616.6	612.5	−4.1	624.7	12.2
100	19.40	3.91	666.0	660.9	−5.1	676.9	16

4. Results and discussion

4.1 SCR-HP system influence on the engine performance

To study the influence of the SCR-HP system on the considered marine two-stroke diesel engine performance, the following three case studies were investigated for engine loads 25%, 50%, 75% and 100% loads: (a) engine without SCR system operating with HS fuel complying with the Tier II NOx limits; (b) engine with the SCR system installed operating with LS fuel complying with the Tier III NOx limits, and; (c) engine with the SCR system installed operating with HS fuel complying with the Tier III NOx limits. It was assumed that the HS and the LS fuels have the same lower heating value.

The derived simulation results are presented in **Fig. 10** and in **Table 5**. It is deduced that the engine with the SCR system installed (operating either with HS or LS fuel) results in higher engine specific fuel oil consumption (SFOC) at all loads, with the additional SFOC (ΔSFOC) being pronounced for the 25% load. For the engine with the SCR-HP system installed, the HS fuel operation (case study (c)) resulted in slightly higher engine SFOC. This behaviour is justified by considering the derived performance parameters presented in **Table 5**. The setting value of the required minimum temperature T_{set} when using HS fuel is about 40°C higher than the T_{set} when using LS fuel. Hence, for the case of the HS fuel, the CBV opens (ϕ_{CBV} increases by reducing the engine loading), resulting in higher cylinder bypass air flow rate. For the case of the LS fuel, the CBV opens only at 25% load achieving an opening of 13.8%, compared to 42.8% for the HS fuel operation. It must be noted that the exhaust gas receiver temperature depends on the ambient temperature (lower ambient temperature results in lower exhaust gas temperature). Thus, the CBV opening also depends on the ambient temperature (lower ambient temperature is expected to result in greater CBV opening). In this study, the ambient temperature was assumed to be 14.8℃ (as measured in the engine trial).

The following values were predicted for the engine SFOC increase compared to the case study (a) SFOC: 0.3 to 1.59 g/kWh for the case study (b); 0.3 to 2.77 g/kWh for the case study (c). Even for the cases where the CBV valve is closed (LS fuel, 50-100% loads), the engine SFOC increases in comparison with the respective SFOC of the engine without the SCR system.

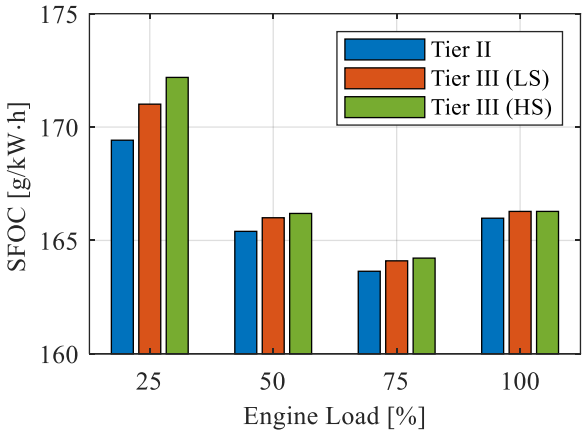

Fig.10 Predicted engine SFOC for the three investigated case studies

Table 5 Simulation results for the case studies (b) and (c)

	LS Fuel					***HS Fuel***				
Load [%]	ΔSFOC [g/kWh]	T_{set} [℃]	$T_{r_{in}}$ [℃]	ϕ_{CBV} [%]	$\dot{m}_{CB}$ [kg/s]	ΔSFOC [g/kWh]	T_{set} [℃]	$T_{r_{in}}$ [℃]	ϕ_{CBV} [%]	$\dot{m}_{CB}$ [kg/s]
25	1.59	285.1	285.1	13.8	0.84	2.77	328.3	328.3	42.8	2.30
50	0.60	290.5	326.6	0	0	0.79	334.7	334.7	3.8	0.39
75	0.46	299.6	339.5	0	0	0.58	345.5	345.5	1.9	0.29
100	0.30	317.7	387.9	0	0	0.30	356.0	387.9	0	0

Fig. 11 provides the cylinders pressure drop and the engine air mass flow rate without the SCR system (case study (a) denoted as Tier II in this figure) and the engine with the SCR system (case study (b) or (c) denoted as Tier III) with the CBV closed. Compared to the Tier II mode, the cylinders pressure drop and air mass flow rate in the Tier III mode decrease (greater reductions are obtained as load reduces). The decrease in the mass of air through the cylinders will cause a decrease in cylinders maximum pressure, which, in turn, causes an increase of the engine SFOC, accordingly. Therefore, the SCR-HP system installation results in increasing engine SFOC and has a greater impact on engine performance at low loads even in cases where the cylinder bypass valve is closed.

When the exhaust gas temperature is lower than the minimum temperature required by the reactor, the CBV opens, and part of the scavenging air is directly bypassed to the turbine inlet, thus affecting the engine performance parameters. **Fig. 12** presents the simulation results of the engine parameters corresponding to various CBV openings (0%, 13.8% and 42.8%) at 25% load for the case study (c). These results are used to analyse the influence of the SCR-HP system and the cylinder bypass on engine scavenging performance. The cylinder bypass causes a drop in the scavenging air pressure resulting to a decrease in the air mass flow rate air through the cylinders, which has an impact on engine performance. The CBV opening leads to a slight increase in the exhaust gas and scavenging air receiver pressures, but the engine cylinder pressure drop (difference between the scavenging air pressure and the exhaust receiver pressure) decreases. With increasing the CBV opening, the cylinder pressure drop becomes smaller, which in turn affects the engine performance (the cylinder scavenging becomes less efficient). The reduction of the cylinders air mass flow rate results in a higher exhaust gas temperature, thus allowing for retaining the exhaust gas temperature above the minimum temperature level required by the SCR reactor operation. However, the CBV opening results in increase of the engine SFOC.

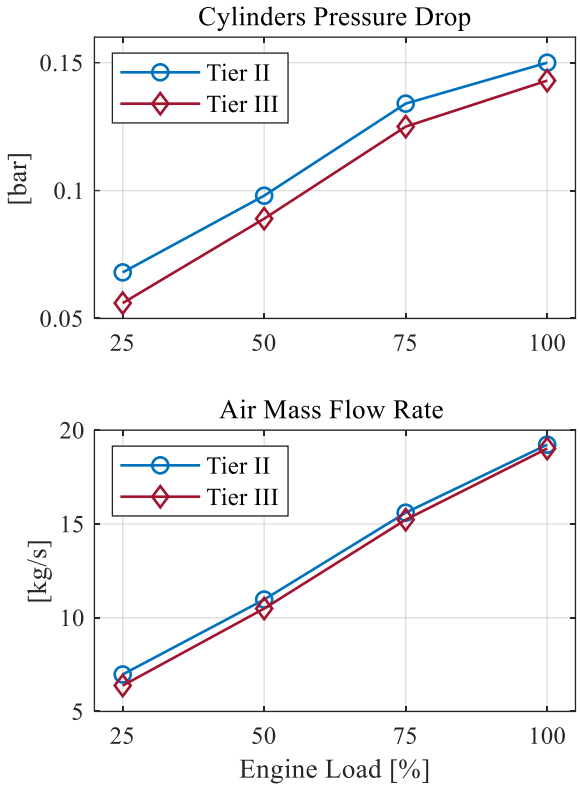

Fig.11 Comparison of the cylinders pressure drop and air mass flow rate for the engine configurations without (Tier II) and with the SCR system (Tier III) assuming closed CBV

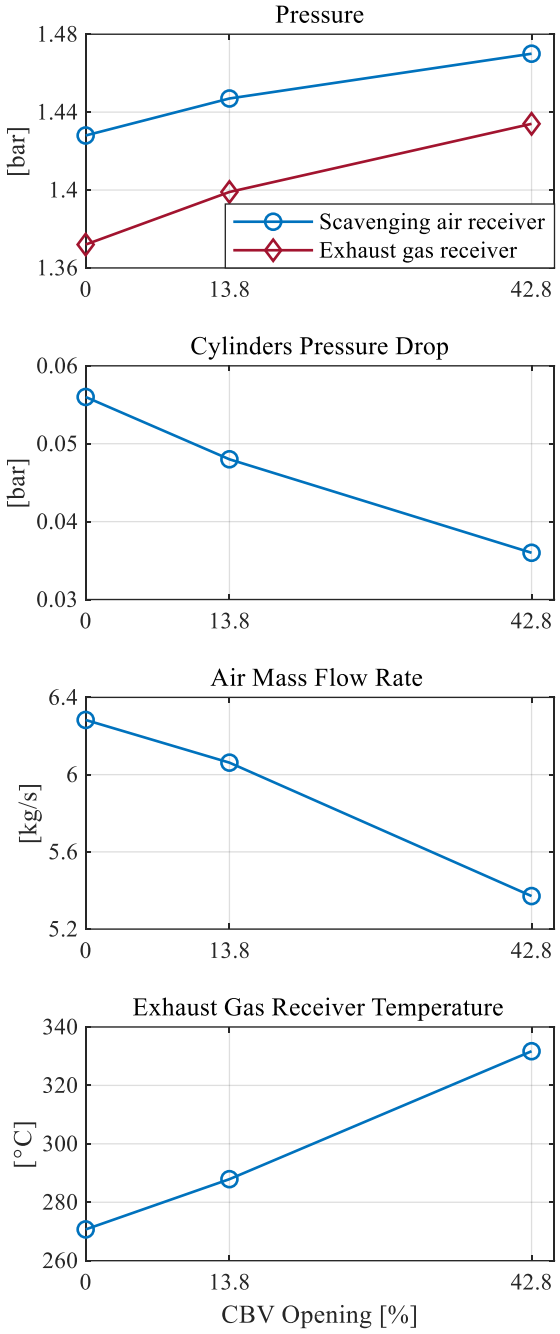

Fig.12 Predicted engine parameters corresponding to CBV openings 0%, 13.8% and 42.8% at 25% load

4.2 Influence of SCR-HP system on engine exhaust gas temperature

The vaporizer and reactor of the SCR-HP system introduce significant thermal and flow inertias between the exhaust receiver and the turbocharger turbine, thus causing the turbocharger delayed response during engine load changes. In this section, the SCR system model was employed to perform simulation runs for all the investigated engine loads to study the influence of the SCR-HP system on the exhaust gas temperature, taking into account a fluctuating exhaust gas temperature term added to the predicted exhaust gas receiver temperature. In this part of the study, it is assumed that the CBV remains closed. The period and amplitude of this fluctuating term was selected to be

1000 s and 20 K, respectively, as such conditions represent a typical dynamic behaviour for the investigated engine in cases of adverse weather conditions according to **Ref. [44,45]**.

The derived simulation results including the exhaust gas temperatures in various locations of the SCR system are presented in **Fig. 13**, where $T_{v_{in}}$ is the vaporizer inlet temperature (equal to the exhaust gas receiver temperature T_e). The reactor inlet temperature $T_{r_{in}}$ exhibits only a slight delay and reduction in the oscillation amplitude compared to the vaporizer inlet temperature. However, the reactor outlet temperature $T_{r_{out}}$ exhibits a significant delay and a reduced oscillation amplitude compared to the vaporizer inlet temperature. This demonstrates that the thermal inertia of the SCR-HP system is mainly caused by the reactor.

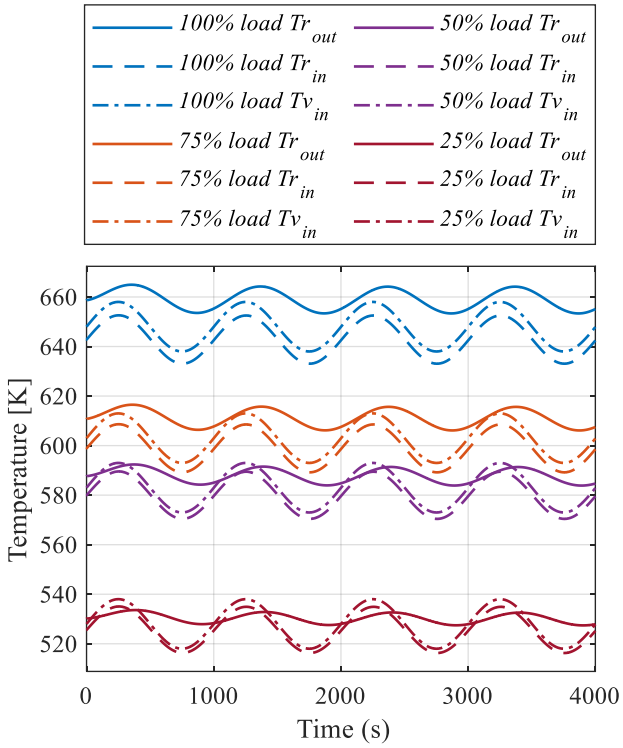

Fig. 13 Derived exhaust gas temperature variation at various locations of the SCR system at 25%, 50%, 75%, 100% loads

The thermal inertia of the reactor is greater than the thermal inertia of the vaporizer, which is mainly attributed to the catalyst block thermal inertia and mass **[44]**. More details reflecting the thermal inertia of the SCR-HP system at 25% load are illustrated in **Fig. 14**, which provides the predicted temperature variations at 25% load including the vaporizer wall temperature T_{v_w}, the reactor wall temperature T_{r_w}, the rector catalyst block temperature $T_{r_{cat}}$. It can be observed that when $T_{r_{in}}$ is higher than $T_{r_{cat}}$, the catalyst block is heated by the exhaust gas (the exhaust gas is cooled), and vice versa. Due to the thermal inertia of the catalyst block, the reactor outlet temperature variation is delayed and its oscillation amplitude is significantly reduced compared to the reactor inlet temperature.

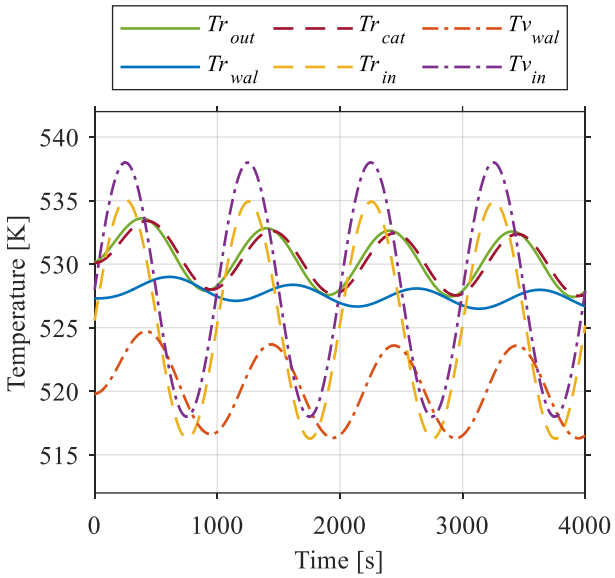

Fig. 14 Predicted temperature variations for the SCR system components at 25% load

Fig. 15 shows the ratios of the fluctuation delay and amplitude reduction of the reactor outlet temperature to the vaporizer inlet temperature. The ratio of the delay time is calculated as the reactor outlet temperature delay time divided by the oscillation period (1000 s). The ratio of the amplitude is calculated as the reactor outlet temperature amplitude divided by the vaporizer inlet temperature amplitude (20 K). It can be observed that as the engine load reduces, the reactor outlet temperature delay increases, whereas the of the reactor outlet temperature amplitude ratio decreases. The temperature delay is greatly affected by the engine exhaust gas mass flow rate **[44]**. Low exhaust gas mass flow rates will slow down the reactor catalyst heating and cooling processes, causing greater delays. It is deduced that at low loads the SCR-HP system has a greater impact on the engine exhaust gas temperature variation, which causes a more delayed turbocharger response. The impact of the SCR-HP system on the engine response at low loads can be mitigated by the appropriate sizing of the electric driven auxiliary blower to retain the required air mass flow.

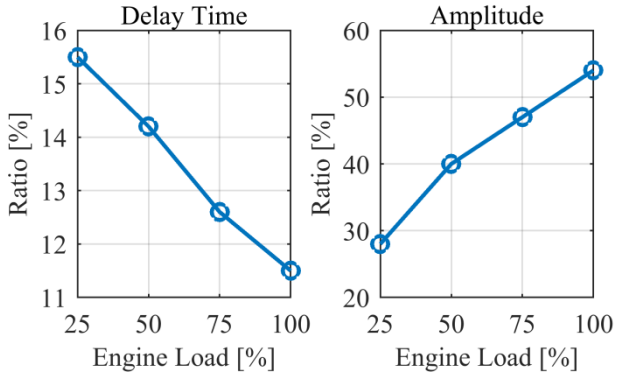

Fig. 15 Ratios of the delay and amplitude reduction of the reactor outlet temperature

4.3 Operation with degraded SCR system components

To investigate the impact the degraded SCR system (a partially clogged reactor as described in Section 2.2.3) on

the engine performance, simulation runs were performed at 25%, 50%, 75% and 100% loads considering the following two case studies: (a) engine with the SCR system using low-sulphur fuel (Tier III (LS)), and; (b) engine with the SCR system using high-sulphur fuel (Tier III (HS)). **Fig. 16** shows the respective percentage differences in various performance parameters as well as the BSFC difference compared to their respective values at healthy conditions (without SCR reactor degradation).

The results demonstrate that the degraded SCR system leads to the reductions of the turbocharger speed (from 1−20%), as well as the scavenging air receiver and exhaust gas receiver pressure, in both case studies (a) and (b) (from 0.5−3.5%, apart from the case of 100% load where a very slight increases in the scavenging and exhaust gas receivers pressures are exhibited). The fouled reactor conditions reduce the engine cylinders difference leading to the air mass flow rate decrease, and thus, the scavenging efficiency deterioration. The compressor and turbine characteristics impact the turbocharger equilibrium and this, the compressor and turbine operating points, which eventually affect the engine performance parameters.

It can be observed from **Fig. 16** that the turbocharger speed reduction becomes greater as the engine load reduces (0.6% reduction at 100% load; reduction greater than 14% at 25% load). The turbocharger speed decrease causes the decrease of the air mass flow rate, which, in turn, leads to the exhaust gas temperature increase. However, the variation trend of exhaust temperature does not completely match that of the air mass flow rate. This is attributed to the reduction of the CBV opening that attenuates the deterioration of engine performance affected by the degraded SCR system. Except for the 25% load of case study (b), the CBV remains closed, as the exhaust gas temperature is higher than the lower limit required at the reactor inlet. The relative change of the CBV opening between the healthy and degraded conditions (shown in **Table 6**) affects the exhaust gas temperature change as well as the BSFC change (greater relative reduction of the CBV opening results in lower increase of the exhaust gas temperature). Thus, the exhaust gas temperature increase is lower for the case study (b) at 25%, 50%, and 75% loads, compared to the same loads of in case study (a). The engine BSFC change (between the healthy and fouled SCR operation) also exhibits similar trends with the exhaust gas temperature.

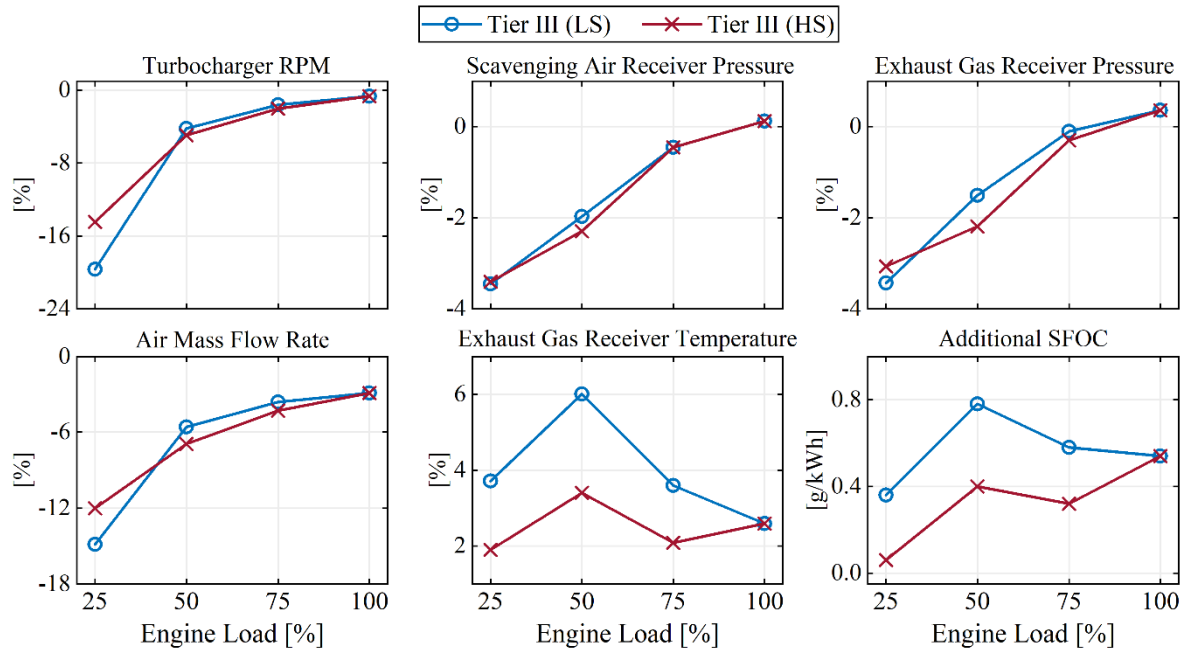

Fig.16 Predicted engine parameters under the SCR reactor degradation

Table 6 CBV opening for the case studies (a) and (b)

	LS Fuel		***HS Fuel***	
Load [%]	Healthy $\phi_{CBV}[\%]$	Degraded $\phi_{CBV}[\%]$	Healthy $\phi_{CBV}[\%]$	Degraded $\phi_{CBV}[\%]$
25	13.8	0	42.8	24.5
50	0	0	3.8	0
75	0	0	1.9	0
100	0	0	0	0

Since the SCR system pressure drop has a significant impact on the marine diesel engines performance, it should be an important performance indicator for the SCR system health. The SCR system pressure drop should be retained to the lowest possible level by implementing appropriate countermeasures.

4.4 Operation with compressor degradation

To investigate the impact of the compressor degradation (described in Section 2.1.3) on the engine and its SCR system performance, simulation runs were performed at 25%, 50%, 75% and 100% loads for the following three cases: (a) engine without the SCR system (Tier II); (b) engine with the SCR system using low-sulphur fuel (Tier III (LS)), and; (c) engine with the SCR system using high-sulphur fuel (Tier III (HS)). The predicted engine performance parameters are presented in **Fig. 17** and **Fig. 18**. The vertical axes of the plots presented in **Fig. 17** represent the percentage change of the parameters from their values at the respective healthy condition (without compressor degradation).

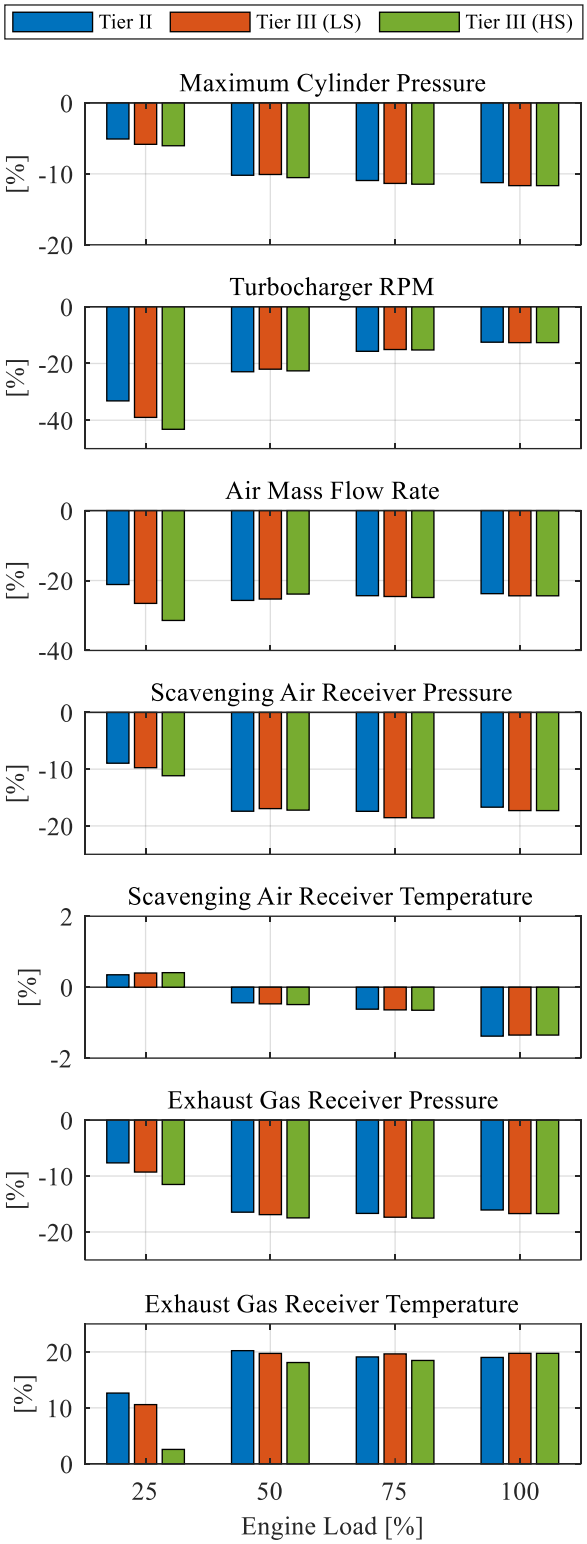

Fig.17 Predicted engine performance parameters under compressor degradation

The results show that the engine performance parameters are significantly affected by the investigated compressor conditions (compressor isentropic efficiency reduced by 20%). This leads to the reduction of the engine receivers pressures, the turbocharger speed and the air mass flow rate, resulting in the reduction of the maximum cylinder pressure, which is associated with the increase of the engine SFOC, as well as the increase of the exhaust gas

receiver temperature. It is observed that the engine parameter changes at 25% load slightly differentiate in comparison with the respective changes at the other operating points (50%, 75% and 100% loads). This is attributed to the operation of the electric driven blower activation, which reduces the impact of the compressor degradation on the engine performance parameters. In the Tier II mode, the compressor degradation caused the air flow decrease by 23.8%, 24.3% and 25.7% at 100%, 75% and 50% load, respectively. As the load decreases, the degree of influence for air flow becomes greater. Due to the effect of the auxiliary blower operation, the air flow reduction rate is only 21.1% at 25% load, which is less than the observed reductions in the other loads.

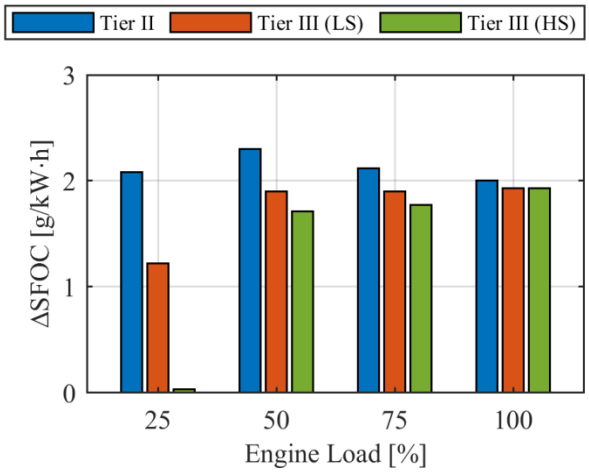

Fig.18 Additional SFOC of the engine under compressor degradation

The engine SFOC increases around 2 g/kWh for 50−100% loads; the configurations with the SCR system result in slightly lower ΔSFOC, which is attributed to the effect of the SCR system energy addition. For the case of 25% load, the engine configurations with the SCR system exhibited a considerably lower ΔSFOC, especially in the case of HS fuel, only a slight increase of 0.04 g/kWh was predicted. For the latter case, the exhaust gas temperature that was found to be higher than the minimum required at the reactor, thus the CBV was kept closed. The compressor degradation results in increasing the exhaust gas temperature, which, in turn, deduces the CBV opening leading to a closed CBV valve in several cases. This causes the attenuation the compressor degradation effect on the engine SFOC.

Fig. 19 presents the reactor inlet temperature $T_{r_{in}}$ and the setting value of the required minimum temperature T_{set} for the reactor for the cases (b) and (c). It can be observed that at all engine loads, $T_{r_{in}}$ is higher than T_{set}, resulting in a complete closing of CBV. As the CVB remains closed, $T_{r_{in}}$ in cases (b) and (c) are equal and the ΔSFOC (originally caused by the cylinder bypass flow) almost zeroes, thus compensating part of the SFOC increase caused by the compressor degradation. In addition, it is worth noting that $T_{r_{in}}$ exceeds the upper NH_3 oxidation limit of 500℃ at 100% load. Therefore, severe compressor degradation may cause the diesel engine exhaust gas temperature to be too high, exceeding the upper limit of the operating temperature of the SCR system.

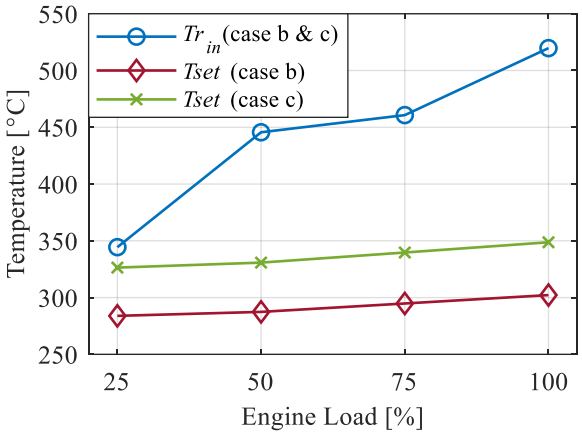

Fig.19 $T_{r_{in}}$ and T_{set} of the reactor under compressor degradation

The cause for the lower ΔSFOC for the cases (b) and (c) (compared with case a) was further analysed. The predicted CBV openings for the case of the engine (without compressor degradation) with the SCR system using LS and HS fuels in Tier III mode are presented in **Table 5**. When $T_{r_{in}}$ is higher than T_{set} due to the compressor degradation, the CBV is completely closed. At 25% load, the CBV opening decrease in case (c) (HS) considerably exceeds the respective CBV opening decrease in case (b) (LS). As a result, the ΔSFOC due to compressor degradation in case (c) is significantly lower than that in case (b), whereas for the Tier II operation (without SCR system), the ΔSFOC exhibits the highest value as the CBV system does not exist. Similar behaviour, but less pronounced, is exhibited at 50% and 75% loads.

5. Conclusions

This study investigated the operation of a large marine two-stroke engine with the selective catalytic reduction (SCR) system for various healthy and degraded conditions by employing an integrated model that sufficiently represents the engine components, the high pressure SCR (SCR-HP) system components and the cylinder bypass valve (CBV) block. The engine model employed the zero-dimensional approach and was validated against the engine experimental data. The SCR-HP system model sufficiently represented this system operation as revealed from its validation against measured data reported in the pertinent literature. The CBV block was modelled to control the cylinder bypass flow for retaining the SCR reactor inlet temperature above its required minimum level. The setting value of the required reactor minimum temperature was calculated based on the exhaust gas pressure and fuel sulphur content to realistically represent the actual SCR system operation. The SCR reactor clogging and the compressor fouling were investigated to identify their impact on the engine performance. The main findings of this study are summarised as follows.

The derived results demonstrated that for the engine equipped with the SCR system, the engine specific fuel oil consumption (SFOC) increased in the range 0.3−1.59 g/kWh for the case of low sulphur fuel, whereas the corresponding SFOC increase was 0.3−2.77 g/kWh for the case of high sulphur fuel. The SFOC increase was more pronounced at low loads, where the cylinder bypass valve opening is adjusted, so that the exhaust gas temperature reaches the reactor minimum temperature set point, which depends on the sulphur content.

The reactor outlet temperature exhibited a significant delay and a reduced oscillation amplitude compared to the reactor inlet temperature; the thermal inertia of the SCR-HP system is mainly attributed to the reactor. At low loads, the SCR-HP system has a greater impact on the engine exhaust gas temperature variation, causing a more delayed turbocharger response. The impact of the SCR-HP system on the engine response at low loads can be mitigated by the appropriate sizing of the electric driven auxiliary blower to retain the required air mass flow.

The SCR reactor partial clogging introduced a pressure drop, which caused the increase of the engine SFOC and the exhaust temperature. The effect will be attenuated due to reduction of the CBV opening, which is more pronounced when the engine operates using high-sulphur fuel. The SCR system pressure drop is an important performance indicator and must be retained to the lowest possible level by implementing appropriate countermeasures.

The compressor degradation reduces the cylinders air flow rate, thus increasing the exhaust gas temperature, which causes the reduction of the CBV opening, and partially mitigates the SFOC increase for the case of the engine equipped with the SCR system. At 25% load, the engine SFOC increased by 0.04 g/kWh for the high sulphur fuel, whereas the respective increase was 2.08 g/kWh for the engine without the SCR system. At 100% load, the compressor degradation may cause the SCR reactor inlet temperature to exceed the upper limit of 500°C (which is required for the normal reactor operation), thereby reducing the SCR reactor effectiveness.

This study supports the better understanding of the operating characteristics of marine two-stroke diesel engines equipped with the SCR-HP system and quantification of the components degradation impact on the engine performance. Moreover, it provides insights for the structural optimisation of the SCR-HP system and the control of marine two-stroke diesel engines equipped with the SCR-HP system. Furthermore, the developed model can be used for the development of the engine room simulator.

Acknowledgements

This work was supported by the China Scholarship Council (grant number 201906575028); and Intelligent Ship Testing and Verification (grant number 2018/473).

The second author greatly acknowledges the funding from DNV AS and RCCL for the Maritime Safety Research Centre establishment and operation. The opinions expressed herein are those of the authors and should not be construed to reflect the views of DNV AS and RCCL.

References

[1] United Nations, 2017. Review of Maritime Transport. United nations conference on trade and development.

[2] Zhang, C.F., et al., 2019. Optimisation design of SCR mixer for improving deposit performance at low temperatures. Fuel. 237, 465–474.

[3] Chen, W.S., et al., 2019. Mechanism and Performance of the SCR of NO with NH3 over Sulfated Sintered Ore Catalyst. Catalysts. 9(1), 90.

[4] International Maritime Organization. 2008. Annex VI of MARPOL 73/78, Regulations for the Prevention of Air Pollution from Ships and NOx Technical Code; International Maritime Organization: London, UK.

[5] Gu, Y.W., and Wallace, S.W., 2017. A potentially overestimated compliance method for the Emission Control Areas. Transp. Res. Part D. 55, 51-66.

[6] International Maritime Organization. 2017. Report of the Marine Environment Protection Committee on Its Seventy-First Session, Annex 1 Resolution MEPC.286(71), (Designation of the Baltic Sea and the North Sea Emission Control Areas). International Maritime Organization: London, UK.

[7] Praveena, V. and Martin, M.L.J., 2018. A review on various after treatment techniques to reduce NOx emissions in a CI engine. J. Energy Inst. 91(5), 704-720.

[8] Gholami, F., et al., 2020. Technologies for the nitrogen oxides reduction from flue gas: A review. Fuel. 714.

[9] Gan, H.B., et al., 2020. Parametric investigation of pre-injection on the combustion, knocking and emissions behaviour of a large marine four-stroke dual-fuel engine. Fuel. 281.

[10] Wärtsilä. 2017.Wärtsilä Environmental Product Guide. 11-25.

[11] Lamas, M.I., et al., 2013. Internal modifications to reduce pollutant emissions from marine. A numerical approach engines. J. Nav. Archit. Ocean Eng. 5, 493–501.

[12] Seddiek, I.S. and Elgohary, M.M., 2014. Eco-friendly selection of ship emissions reduction strategies with emphasis on SOx and NOx emissions. J. Nav. Archit. Ocean Eng. 6, 737–748.

[13] Späth, N. DNV GL releases updated DNV GL NOx TIER III compliance guide; Available from: https://www.dnvgl.com/news/dnv-gl-releases-updated-dnv-gl-nox-tier-iii-compliance-guide-98168. [Accessed 2020-08-17]

[14] Wik, C. and Niemi, S., 2016. Low emission engine technologies for future tier 3 legislations options and case studies. J Shipping Trade. 1(1), 1–22.

[15] Wang, D.W., et al., 2020. Numerical and thermodynamic study on effects of high and low pressure exhaust gas recirculation on turbocharged marine low-speed engine. Appl. Energy. 261.

[16] Vignesh, R. and Ashok, B., 2020. Critical interpretative review on current outlook and prospects of selective catalytic reduction system for De-NOx strategy in compression ignition engine. Fuel. 276.

[17] MAN B&W. 2019. MAN emission project guide: MAN B&W two-stroke marine engines. MAN B&W press, Copenhagen.

[18] Uma, H.S., et al., 2019. Numerical study on the design of urea decomposition chamber in LP SCR system. J. Nav. Archit. Ocean Eng. 11, 307–313.

[19] Zhang, L., et al., 2019. Recent advances in the preparation of zeolites for the selective catalytic reduction of NOx in diesel engines. React. Chem. Eng. 4, 975-985.

[20] Li, Y.L., et al., 2020. Hierarchical three-dimensionally ordered macroporous Fe-V binary metal oxide catalyst for low temperature selective catalytic reduction of NOx from marine diesel engine exhaust. Appl. Catal. B-Environ. 268.

[21] Wang, Z.Y., et al., 2019. Nitrogen Oxide Removal by Coal-Based Activated Carbon for a Marine Diesel Engine. Appl. Sci. 9(8),1656.

[22] Cho, C.P., et al., 017. NOx reduction and N_2O emissions in a diesel engine exhaust using Fe-zeolite and vanadium based SCR catalysts. Appl. Therm. Eng. 110, 18–24.

[23] Jung, Y., et al., 2017. NOx and N_2O emissions over a Urea-SCR system containing both V_2O_5 -WO_3 /TiO_2 and Cu-zeolite catalysts in a diesel engine. Chem. Eng. J. 326, 853–862.

[24] Wang, Z.G., et al., 2020. Reaction mechanism and chemical kinetics of NH_3-NO/NO_2-SCR system with vanadium-based catalyst under marine diesel exhaust conditions. 234(3), 342-352.

[25] Ye, D., et al., 2016. Investigation of the promotion effect of WO3 on the decomposition and reactivity of NH4HSO4 with NO on V_2O_5-WO_3/TiO_2 SCR catalysts. RSC Adv. 6, 55584–55592.

[26] Zhu, Y.Q., et al., 2019. Ammonium-salt formation and catalyst deactivation in the SCR system for a marine diesel engine. Catalysts. 9(1), 21.

[27] Zhu, Y.Q., et al., 2018. Influences of NH_4NO_3 on the NOx reduction pathways with vanadium-based catalyst under diesel exhaust conditions. Russian J Phys Chem A. 92, 1473–1480.

[28] Xi, H.Y., et al., 2019. New experimental results of NO removal from simulated marine engine exhaust gases by $Na_2S_2O_8$/urea solutions. Chem. Eng. J. 362, 12–20.

[29] Nielsen, J.B. and Pedersen, E., 2019. A system approach to selective catalyst reduction DeNO(x) monolithic reactor modelling using bond graphs. P I MECH ENG M-J ENG. 233(2), 632–642.

[30] Moon, S.J., et al., 2014. Numerical prediction on the influence of mixer on the performance of urea-SCR system. Waste Int J Mech Aero Ind Mechatron. 8(5), 972–978.

[31] Choi, C., et al., 2015. Numerical analysis of urea decomposition with static mixers in marine SCR system. J Clean Energy Technol. 3(1), 39–42.

[32] Woschni, G., 1967. A Universally applicable equation for the instantaneous heat transfer coefficient in the internal combustion engine, SAE Paper no 670931.

[33] Ghojel, J.I., 2010. Review of the development and applications of the wiebe function: A tribute to the contribution of Ivan Wiebe to engine research. Int J of Engine Res. 11(4), 297-312.

[34] Zhu, Y.Q., Zhang, R., Zhou, S., et al., 2019. Performance optimization of high-pressure SCR system in a marine diesel engine. Part I: Flow Optimization and Analysis. Topics in Catalysis. 62, 27–39.

[35] Zhu, Y.Q., Zhang, R., Zhou, S., et al., 2019. Performance optimization of high-pressure SCR system in a marine diesel engine. Part II: catalytic reduction and process. Topics in Catalysis. 62, 40–48.

[36] Sung, Y., et al, 2020. Synergistic effect of mixer and mixing chamber on flow mixing and NOx reduction in a marine urea-SCR system. Chem. Eng. Process.150.

[37] Yu, B., 2016. Numerical simulation study on optimal layout of static mixer in SCR denitration system. Comput Appl Softw. 33(12), 60–62.

[38] Choi, C., et al., 2015. Numerical analysis of NOx reduction for compact design in marine urea-SCR system. J. Nav. Archit. Ocean Eng. 7, 1020–1033.

[39] Zhanga, C., et al., 2019. Optimisation design of SCR mixer for improving deposit performance at low temperatures. Fuel. 237, 465–474.

[40] Chen, P. and Wang, J., 2014. Control-Oriented Model for Integrated Diesel Engine and Aftertreatment Systems Thermal Management. Control Eng. Pract. 22, 81–93.

[41] Chen, P. and Wang, J., 2012. Control-Oriented Modeling and Observer-Based Estimation of Solid and Gas Temperatures for a Diesel Engine Aftertreatment System. ASME J. Dyn. Syst. Meas. Control. 134(6), 061011.

[42] Park, T., et al., 2014. Effect of static mixer geometry on flow mixing and pressure drop in marine SCR applications. J. Nav. Archit. Ocean Eng. 6(1), 27–38.

[43] Pedersen, N., et al., 2016. FMI for Co-Simulation of Embedded Control Software. In Proceedings of the 1st Japanese Modelica Conference (pp.70-77). Linköping University Electronic Press. (Linköping Electronic Conference Proceedings; No. 124).

[44] Foteinos, M.I., et al., 2019. Simulation of the Transient Thermal Response of a High Pressure Selective Catalytic Reduction Aftertreatment System for a Tier III Two-Stroke Marine Diesel Engine, J ENG GAS TURB POWER. 141, 071001-1.

[45] Foteinos, M.I., et al., 2020. Response of a direct-drive large marine two-stroke engine coupled to SCR exhaust aftertreatment system when operating in waves, P I MECH ENG M-J ENG. 234(3), 651-667.

[46] Zhu, Y.Q., et al., 2020. Combustion and emission characteristics for a marine low-speed diesel engine with high-pressure SCR system. Environ Sci Pollut Res. 27, 12851–12865.

[47] Tang, Y. and Zhang, J., 2017. Development of a real-time two-stroke marine diesel engine model with in-cylinder pressure prediction capability. Appl. Energy. 194, 55-70.

[48] Benson, R.S., 1977. A new gas dynamic model for the gas exchange process in two stroke loop and cross scavenged engines. Int J Mech Sci. 19(12), 693–711.

[49] Sigurdsson, E., 2011. Scavenging Flow in a Two-Stroke Diesel Engine. University of Denmark.

[50] Dang, D. and Wallace, F.J., 1992. Some single zone scavenging models for two-stroke engines. Int J Mech Sci. 34(8), 595–604.

[51] Tang, Y. and Zhang, J., 2017. Investigating the effect of cylinder body on the accuracy of marine diesel engine model. J Harbin Eng Univ. 38(12), 1836-1843.

[52] Xiang, L., et al., 2019. Investigation on Gaseous Fuels Interchangeability with an Extended Zero-dimensional Engine Model. Energ Convers Manage. 183, 500-514.

[53] Theotokatos, et al., 2018. Development of an extended mean value engine model for predicting the marine

two-stroke engine operation at varying settings. Energy. 143, 533-545.
[54] Shen, H., et al., 2020. Development of a Marine Two-Stroke Diesel Engine MVEM with In-Cylinder Pressure Trace Predictive Capability and a Novel Compressor Model, J. Mar. Sci. Eng. 8(3), 204.
[55] Ntonas, K., et al., 2020. Integrated Simulation Framework for Assessing Turbocharger Fault Effects on Diesel-Engine Performance and Operability. J ENERG ENG. 146(4).
[56] Heywood, J.B., 1988. Internal combustion engine fundamentals. McGraw-Hill.
[57] Galindo, J., et al., 2013. Characterization of a radial turbocharger turbine in pulsating flow by means of CFD and its application to engine modeling. Appl. Energy. 103, 116–27.
[58] Watson, N. and Janota, M.S., 1982. Turbocharging the internal combustion engine. London: Macmillan.
[59] Theotokatos, G. and Tzelepis, V., 2015. A computational study on the performance and emission parameters mapping of a ship propulsion system. Proc Inst Mech Eng Part M-J Eng Maritime Environ. 229, 58–76.
[60] Shen, H. and Zhang, J., 2020. Applicable and Comparative Research of Compressor Mass Flow Rate and Isentropic Efficiency Empirical Models to Marine Large-Scale Compressor. Energies. 13(1), 47.
[61] Tsinoglou, D.N., et al., 2004. Transient Modelling of Flow Distribution in Automotive Catalytic Converters. Appl Math Model. 28(9), 775–794.
[62] Xiao, Y., et al., 2019. Investigation on the Control Strategy for Marine Selective Catalytic Reduction System. J DYN SYST-T ASME. 141(1).
[63] Tang, Y., 2018. Research on The Modeling Methods of Power Engine for Marine Engine Room Simulator. Dalian Maritime University.
[64] Hountalas, D.T., 2000. Prediction of marine diesel engine performance under fault conditions, Appl. Therm. Eng. 20(18), 1753–1783.
[65] Nahim, H.M., et al., 2016. Oriented review to potential simulator for faults modeling in diesel engine. J. Mar. Sci. Technol. 21(3), 533-551.
[66] Rubio, J.A.P., et al., 2018. Marine diesel engine failure simulator based on thermodynamic model. Appl. Therm. Eng. 144, 982–995.
[67] Alegret, G., et al., 2015. Modeling of a Large Marine Two-Stroke Diesel Engine with Cylinder Bypass Valve and EGR System. IFAC. 48(16), 273-278,